Received: March 24, 2015 Revised: July 23, 2015 Accepted: August 17, 2015

(onlinelibrary.wiley.com) DOI: 10.1111/ner.12350

Automated Segmentation and Reconstruction of the Subthalamic Nucleus in Parkinson's Disease Patients

Bo Li, PhD*; Changqing Jiang, PhD*; Luming Li, PhD*†; Jianguo Zhang, MD‡; Dawei Meng, MD‡

Objective: In the treatment of Parkinson's disease for deep brain stimulation (DBS), the subthalamic nucleus (STN) is the most important target on a specific brain nucleus. Although procedural details are well established, targeting STN remains problematic because of its variable location and relatively small size.

Materials and Methods: Data were collected from 10 patients with Parkinson's disease implanted with deep brain stimulation devices. This paper presents an automated algorithm for 3.0T magnetic resonance (MR) image segmentation using the level set method to reconstruct the STN based on automatic segmentation. Implicit polynomial surfaces are used for the reconstruction of the STN segmentation.

Results: The method was applied to 10 Parkinson's disease (PD) patients to automatically extract and rebuild the STN. A comparison of the Euclidean distances and dice overlap coefficient showed no significant differences with the segmentation-based method, with the present method having smaller prediction errors and being more robust than expert systems.

Conclusions: This paper presents an automated algorithm to segment and reconstruct the small human STN using MR images. This method for STN should provide an effective method for advancing STN localization and direct visualization.

Keywords: Automated segmentation, MRI, Parkinson's disease, reconstruction, subthalamic nucleus

Conflict of Interest: The authors reported no conflict of interest.

INTRODUCTION

High-frequency deep brain stimulation (DBS) of the subthalamic nucleus (STN) is an effective treatment for advanced Parkinson's Diseases (PD) (1). The therapeutic benefits of DBS in reducing motor function-related symptoms are closely related to the placement accuracy of the DBS electrodes in the motor subregion of the STN (2). Secondary side-effects of the stimulation may occur depending on the location and trajectory of the electrodes (3). Medical imaging is usually used to assist the process to better localize the targeted nucleus. Magnetic resonance imaging (MRI) is one of the most commonly used modalities due to its good image contrast and spatial resolution (4,5).

Several anatomical and physiological targeting methods are commonly used for localization of the STN. Anatomical methods include both direct and indirect techniques. Direct targeting involves specific T2-weighted MRI sequences that enable visualization of the STN boundaries (6). The indirect methods are based on brain atlases and typically use the anterior commissure (AC) and the posterior commissure (PC) as internal landmarks to co-register the atlas with the patient, such as the Schaltenbrand–Wahren atlas (7). However, there are several limitations in this method. First, exact localization of the electrode within the STN should provide the best efficacy for PD (8–10), but the STN is not readily visible in conventional MR images. Locating subregions of the STN in the images is even more challenging. Second, the human STN has morphometric variations between individuals (2,11), so localization based on atlases can generate errors from patient to patient. During surgery, the precise stimulation site can be refined using physiological microelectrode recording (MER) (12,13), but repeated MER are necessary to delineate the STN borders. These increase the operation duration as well as the risk of bleeding (14). Therefore, a better way to precisely localize the nucleus is still needed. Segmentation and reconstruction of the STN based on MR imaging can obtain intuitive perspectives of the STN, understand the relationship between therapeutic effect and electrode placements (15), and adapt to individual differences. This can facilitate neurosurgeons to precisely locate preoperative STN and provide clinical guidance for reducing the repeated intraoperative adjustments as well as the risk of bleeding. Thus, MRI can help neurosurgeons obtain more information about the anatomic localization and morphological features to further aid precise localization of the electrode.

Address correspondence to: Luming Li, PhD, National Engineering Laboratory for Neuromodulation, School of Aerospace, Tsinghua University, Beijing 100084, China. Email: lilm@mail.tsinghua.edu.cn

* National Engineering Laboratory for Neuromodulation, School of Aerospace, Tsinghua University, Beijing, China;
† Center of Epilepsy, Beijing Institute for Brain Disorders, Beijing, China; and
‡ Department of Neurosurgery, Beijing Tiantan Hospital, Capital Medical University, Beijing, China

For more information on author guidelines, an explanation of our peer review process, and conflict of interest informed consent policies, please go to http://www.wiley.com/WileyCDA/Section/id-301854.html

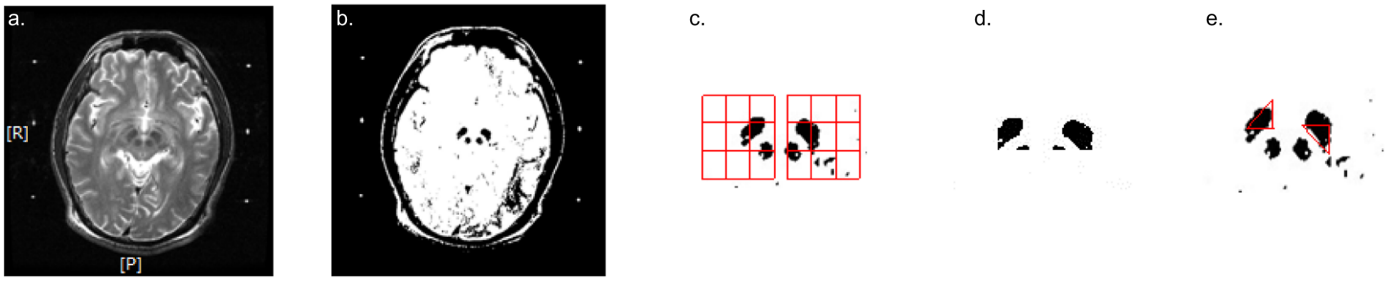

Figure 1. Contour element diagrams. a. Raw image. b. Image binarization. c. and d. Extraction of regions of interest and STN regions. e. Initial contours. R, right; P-posterior. STN, subthalamic nucleus.

There are two main approaches for the segmentation and reconstruction of the STN. The first one relies on manually delineating its contour on individual slices and then reconstructing the STN. Shen et al. (7) visualized an STN using this method. The second is atlas based, with the STN first segmented manually for a subject by experienced experts to form an STN atlas, with another STN then segmented using this atlas through a fusion scheme. Xiao et al. (2,16) used the majority-voting label-fusion method to segment an STN based on an atlas formed by manual segmentations. These methods are based on manual segmentation of the STN, but a presurgery scanner can provide only one MR image with clear STN boundaries in only one direction. This can make accurate segmentation and reconstruction of STN challenging. Although some researchers have attempted visualization analyses (12,13,17,18), there is a lack of automated segmentation and reconstruction methods for the STN based on MRI.

This study investigates automated segmentation and reconstruction of STN directly visualized by 3T T2W MR imaging. The system used automated segmentation based on the level set method to identify the STN instead of manual contour identification. Level set methods are a conceptual framework that use level sets as a tool for numerical analyses of surfaces and shapes that can be easily used to follow shapes that change topology (19–22). The location of the STN in stereotactic space was based on automated reconstruction using automated segmentation to obtain more in-depth and intuitive perspectives of the STN that can provide clinical guidance for effective anatomical localization of the STN.

MATERIALS AND METHODS

MRI Acquisition

Ten patients with PD (six men, four women, 64.1 ± 6.3 years) who were being treated with STN DBS procedures were scanned before surgery. The unified Parkinson's disease scale (UPDRS III) scores were evaluated as 18.80 ± 11.28 and 42.60 ± 20.92 with and without medication. MRI of the brains was performed with a 3.0T MR scanner (GE medical systems, Tiantan Hospital, Beijing, China). The frame-based T2 FSE MRIs (TR = 3140 ms, TE = 97 ms, matrix = 512 × 512, thickness = 3 mm, FOV = 240 mm) included 15 coronal slices and 20 axial slices. Frame-based T1 MRIs were obtained (TR = 6.9 ms, TE = 1.6 ms, matrix = 512 × 512, thickness = 3 mm, FOV = 240 mm, 20 axial slices) to determine the brain space. Twenty microelectrode recordings were obtained from 10 patients undergoing STN implantation for DBS.

Automatically Segmentation Algorithm

The STN was automatically segmented by analyzing the MR image intensity to generate a binary image with the threshold determined by the maximum likelihood estimate (MLE) method (23). A grid including the STN region was set up and labeled on the central zone of the binary image. The initial contour was delineated by the grid and used to begin the STN segmentation using the level set method.

Initial STN Contour

Automatic acquisition of the initial contour was a key step in the algorithm shown in Figure 1. Firstly, because the STN usually appeared as a dark region in the T2-weighted images, the STN could be roughly separated from the surroundings by whole image binarization. The maximal expectation of the intensity of the gray matter, which includes the STN, was determined using the MLE method and used as the initial threshold, T_0. The intensity of each pixel was set to zero if the intensity was less than T_0, otherwise, the

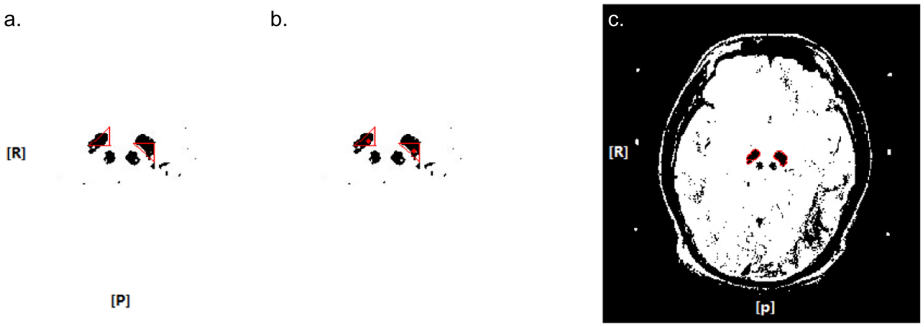

Figure 2. Segmentation identification. a. Extraction of STN regions and the initial contours; b. the initial seeds of region growing method; c. segmentation results of region-growing method. R, right; P, posterior. STN, subthalamic nucleus.

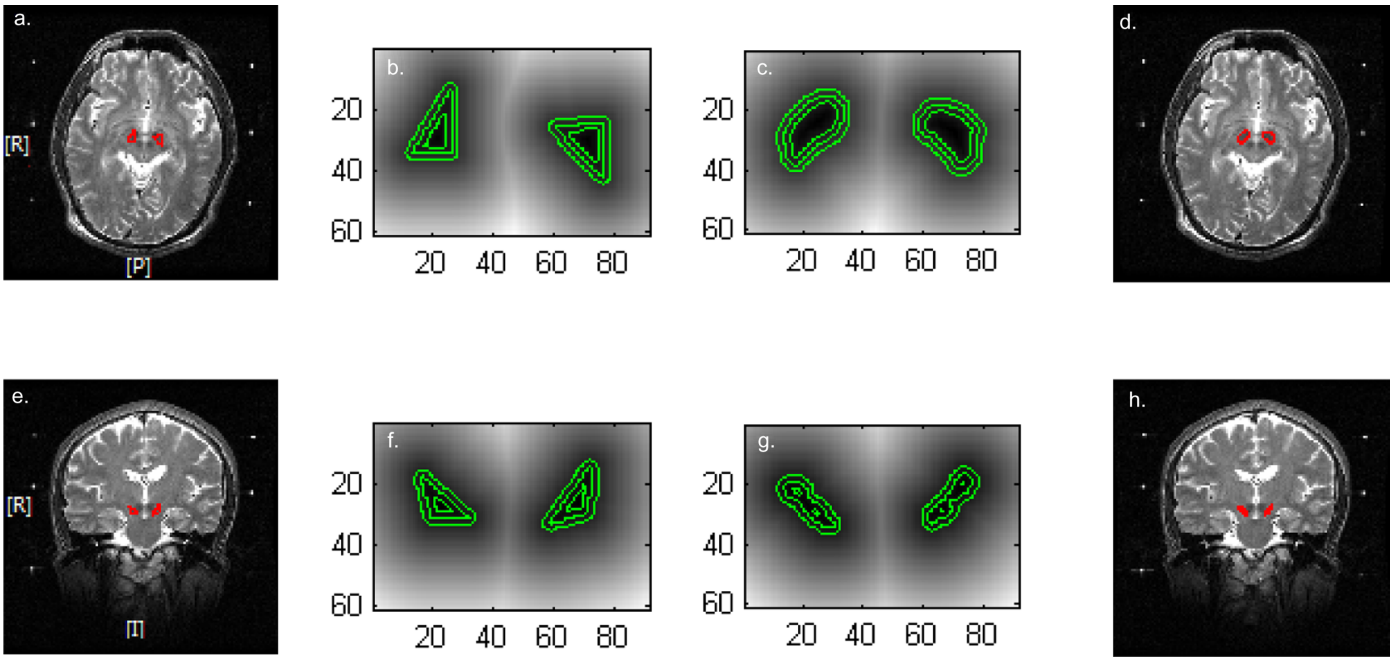

Figure 3. Segmentation of axial and coronal images. a. and e. Raw images. b. and f. Initial level set function at levels −2, 0, 2. c. and g. Final level set function contours. d. and h. Zero-level contours overlaid on the images. R, right; P, posterior; I, inferior.

intensity was set to the maximum. Secondly, the STN region, an m × n grid, was then extracted according to the morphological characteristics. The region area, S, consisting of all pixels with intensities of zero, was then calculated. For any i ∈ [1,m], j ∈ [1,n], the average density of region(i, j), $N_{i,j}$, was the total number of pixels in that region with an intensity of zero. Subregion(i, j) was labeled 1 if $N_{i,j} \geq N$, N being the average intensity of the entire set to identify the subregion which includes the STN boundaries, otherwise, subregion(i,j) was labeled −1. The red nuclei (RN) regions could be extracted from the relative positions of the RN and STN. Finally, for any i ∈ [1, m], j ∈ [1, n], an element, $I_{i,j}$, of the initial contour I was determined as $I_{i,j}$ belonged to the initial contour if either $I_{i-1,j}$ or $I_{i+1,j}$ was of opposite signs or $I_{i,j-1}$and $I_{i,j+1}$are of opposite signs. The center of $I_{i,j}$ represented the element position, so the center belonged to the initial contour point set. The initial contour I included the right contour I_r and the left contour I_l. If I_r or I_l was Φ, the above steps were repeated until both I_r and I_l were not Φ. All the points in I formed the initial contour C. The center of the set I_r and I_l were used as seeds and the STN region in the binary image was obtained using region-growing method (24) in Figure 2. The right STN area S_r in the binary image was the sum of all pixels in the right STN region and the left STN area S_l was the sum of all pixels in the left STN region. The right and left STN areas were taken as standards to judge the final segmentation results.

Level Set Method

The final STN contour was found using the level set method. Chan and Vese (21) used a model for active contours (CV model) to detect objects in a given image through minimizing the Mumford–Shah

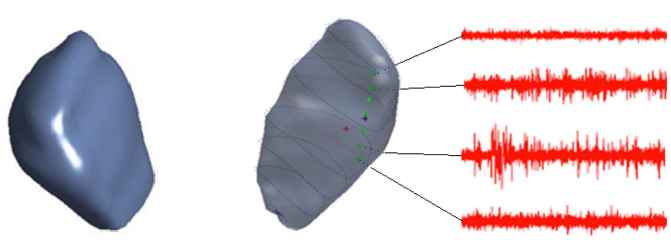

Figure 4. Front views of the reconstructed STN and STN targets. The red point is the expert's STN target. The green points show the MER locations from 2.5 mm to about 0.5 mm below the red point in left STN with the electrode finally located 0.5 mm below. Intraoperative testing showed that the therapeutic benefits were significantly improved with no obvious side-effects. The black point is the target given by the present method. The intersection angle between the electrode trajectory and the AC-PC plane was about 60 degrees while that relative to median sagittal plane was about 15 degrees. AC, anterior commissure; MER, microelectrode recording; PC, posterior commissure; STN, subthalamic nucleus.

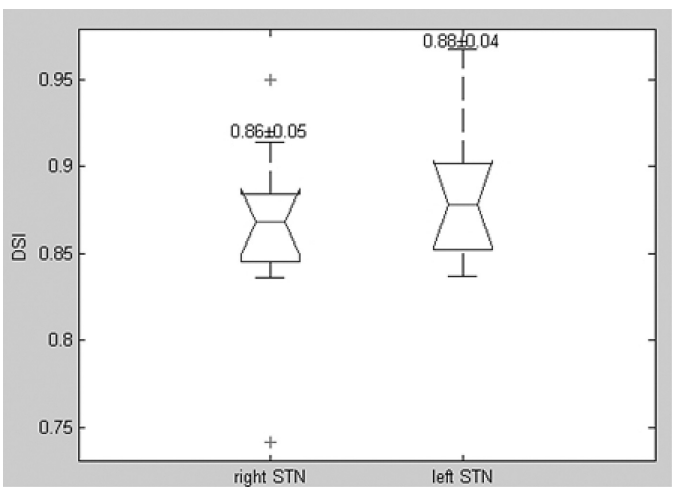

Figure 5. Dice overlap coefficient.

Table 1. Position Coordinates Given by the MER, Expert, and Automatic Segmentation.

STN	MER		Expert		Present method	
	Right	Left	Right	Left	Right	Left
Lateral (mm)	13.4 ± 1.2	11.7 ± 1.6	13.2 ± 1.3	11.3 ± 1.7	13.2 ± 1.3	11.5 ± 1.5
AP (mm)	2.6 ± 1.1	2.7 ± 1.1	2.6 ± 1.1	2.7 ± 1.1	2.6 ± 1.0	2.8 ± 1.1
Vertical (mm)	4.2 ± 2.4	4.0 ± 2.5	5.1 ± 2.1	5.1 ± 2.2	3.8 ± 2.1	3.9 ± 2.3

MER, microelectrode recording; STN, subthalamic nucleus.

functional for segmentation. The CV model used a narrow limited (NL) method for localizing active contours to interact with one another to segment the image (22). Let $\Omega \subset R^2$ be an image domain and $I : \Omega \to R$ be a given image. Let $\phi : \Omega \to R$ be a level set function on the domain Ω. Let $R(x, y)$ mask a narrow band region which will be 1 when point y is within a ball of the radius R centered at x, otherwise 0. An energy function was defined as in the Lankton method as

$$E(\phi) = \int_{x\in C}\int_{y\in\Omega_y} R(x,y)F_x(y,u_1',u_2')dydx + \mu\int_{x\in C}\|\nabla\phi(x)\|dx \quad (1)$$

where $F_x(y,u_1',u_2') = |I(y_{in(c)} - u_1')|^2 + |I(y_{out(c)} - u_2')|^2$ is the generic internal energy, u_1' is the intensity mean of the interior of level contour C within $R(x, y)$, u_2' is the intensity mean of the exterior of the level contours, and $\mu > 0$ is a constant. The second term kept the contour smooth.

A double-well potential function (25) was used to ensure the accuracy of the curve and to keep the narrow band smooth,

$$p(x) = \begin{cases} \frac{1}{(2\pi)^2}(1-\cos(2\pi x)), 0 < x \le 1 \\ \frac{1}{2}(x-1)^2, x > 1 \end{cases} \quad (2)$$

The energy function in Equation (1) can then be changed to:

$$E(\phi) = \int_{x\in C}\int_{y\in\Omega_y} R(x,y)F_x(y,u_1',u_2')dydx + \mu\int_{x\in C} p(|\nabla\phi(x)|)dx \quad (3)$$

The energy function was minimized with respect to ϕ by calculating the gradient flow function using the standard gradient descent method to calculate the level set function with the zero level contours as the boundaries of the segmentation results. When the right or the left area of the result was less than the area in same side of the binary image, the above steps were repeated. When both side areas of the result were greater than the area in same side of the binary image, the result was the final automatic segmentation.

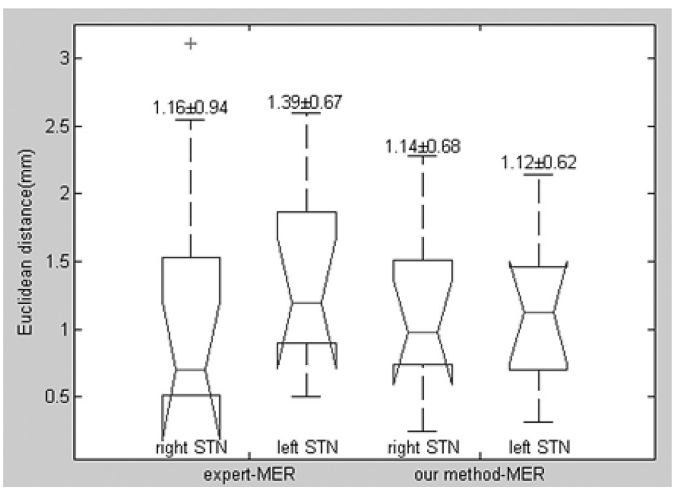

Figure 6. Euclidean distance validation.

Three-Dimensional Reconstruction of the STN

The three-dimensional reconstruction process included automatic segmentation, registration, interpolation, and reconstruction of the STN. First, the STN contours were established on the axial and coronal slices using the automated segmentation and matched using the landmarks of the stereotactic frame. Second, the STN contours on the axial slices were interpolated relative to the minor axis of the STN on the coronal slice along the z-coordinate direction. Finally, the contours on the axial slices were reconstructed using the level set method by fitting implicit polynomial surfaces (26).

Evaluation of the Automatic Segmentation and Reconstruction Method

The segmentation and reconstruction depend on the choice of the coordinate space. In stereotactic neurosurgeries, the commissure points are frequently used as landmarks to infer the location of the subcortical structures. The midpoint of the anterior commissure (AC) and the posterior commissure (PC) is viewed as an origin in the coordinate system. The x-coordinate is defined as the lateral-medial distance, the y-coordinate as the anterior-posterior distance, and the z-coordinate as the superior-inferior distance. Fame-based coordinates were transformed into AC-PC coordinates as a way to correct for frame placement and to compare different patients.

The automatic segmentation method was used to delineate and reconstruct the STN. The results compared with MER of the STN as the gold standard. The automatic and manual segmentations were evaluated based on: 1) the position of the STN targets with the expert and automatic segmentation; and 2) the Euclidean distances between the positions in the MER and the automatic segmentation between the positions in the MER and manual segmentation. In addition, the dice overlap coefficient is defined as: $\mathrm{DSI} = \frac{2|S \cap T|}{|S|+|T|}$, where $|S|$ and $|T|$ denote the number of pixels in the manual and automatic segmentation and $|S \cap T|$ denotes the number of pixels in the overlay of the two segmentation results (2,7).

RESULTS

Automatic Segmentation and Reconstruction of the STN

The axial and coronal image segmentation results from our method are shown in Figure 3. The green curves (Fig. 3b,f) are the initial contours while the red curved regions (Fig. 3d,h) are the final

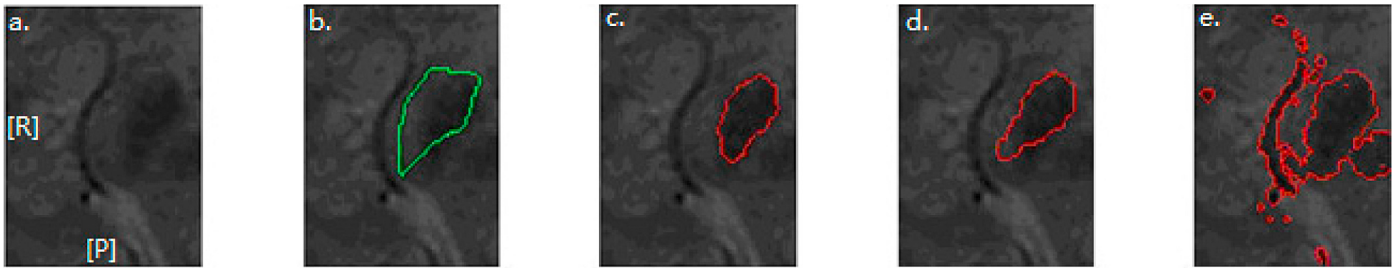

Figure 7. Comparison of results from various algorithms. a. Raw image. b. Initial contour. c. Segmentation result of present method. d. NL result. e. CV result. NL, narrow limited.

segmentation results. In Figure 3c,g are plots of the final level set function after the evolution while the black contours are the zero-level contours of the level set function. Figure 4 shows the three-dimensional view of the reconstructed STN in AC-PC aligned space. The morphological features of the STN on the brain can be visualized directly in three-dimensional space. The dice overlap coefficient of the right STN between the manual and automatic segmentation results shown in Figure 5 is 0.86 ± 0.05 while the left STN is 0.88 ± 0.04.

The axial and coronal image segmentation results show the STN position in three dimensions. These coordinates were then translated into the AC-PC aligned space. The patients were also analyzed by an expert to select the STN. The STN target position is an important measurement for the segmentation results. Starr (27) gave the position as 12 mm lateral, 2 mm posterior, and 4 mm inferior to the MC point as the center of STN in brain space. The average STN positions given by the various methods are listed in Table 1. The average positions are more lateral and more posterior in the brain space than the MER location. The Euclidean distance in Figure 6 shows no statistical significance ($p = 0.47$), with our method having smaller prediction errors than the expert.

DISCUSSION

STN-DBS surgery has been accepted as a long-term therapeutic option for patients with advanced PD. A therapeutic outcome largely relies on accurate localization of this lead. However, this procedure remains challenging for neurosurgeons because of the small size of the target deep inside the human brain that is surrounded by various vital structures (13). Automatic segmentation and reconstruction of the STN using 3T MRI can provide direct visualization and increase target precision. Therefore, it may be helpful for the neurosurgeons to automatically locate preoperative STN, better perform the surgery, and reduce the repeated intraoperative adjustments as well as the risk of bleeding.

Figure 7 compares the present method with results of the NL method (22) and the CV model (21). Figure 7a shows the raw image while Figure 7b shows the initial contour. Figure 7c shows the segmentation result of the current method while Figure 7d shows the NL method result. Their result is obtained when each point on the curve is located such that the local interior and exterior about each point along the curve minimizes the energies in the local region (21). Their method uses distance regularization to move every point forward and backward along the curve. Figure 7e shows the result of the global CV model that is very sensitive to the edge position. The CV model leads to a false segmentation because the STN region intensity is not constant and the STN edge is not distinct. The results show that the current method is more effective than the other methods.

Automatic Segmentation

The results show that the method is robust to the initial curve placement. The initial contours may cross and go beyond the

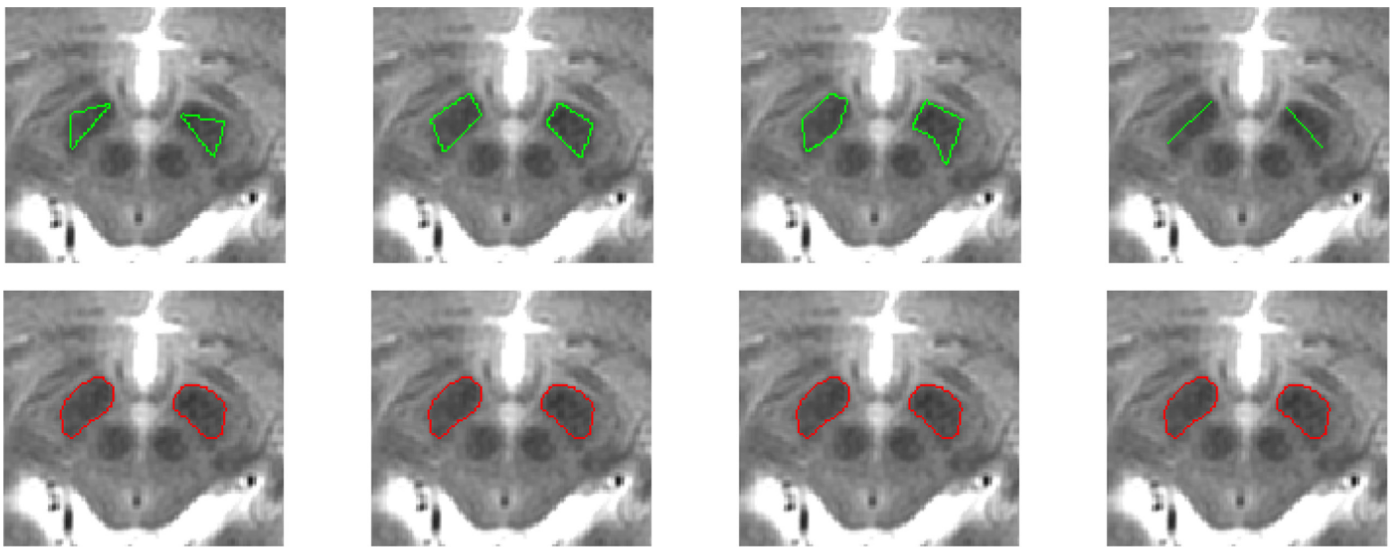

Figure 8. Comparison of segmentation results based on various initial contours.

boundaries of the STN or even contain obvious edges from neighboring nuclei. The method in this paper uses the level set method to segment the STN region from human brain MR images using an arbitrary initial shape that is related to the image intensity, such as a triangle, a quadrangle, a pentagon, and a line. The red curves in Figure 8 are the segmentation results. During the contour evolution, the contours expand and shrink until they stop at the right boundaries. The analysis and dice overlap coefficients in Figure 5 show that the method is quite robust.

STN Visualization

There have been many reports on visualization of the STN. However, these reports were all based on manual segmentation of the STN which takes much time and labor. The STN DBS can have side-effects depending on the location and trajectory of the electrodes because the DBS are implanted to the dorsolateral (motor) part of the STN (3,28). Presurgery scanners acquire limited axial slices with clear STN boundaries, but they do not give enough information to precisely reconstruct the STN by manual method (7) and atlas-based method (2,11). High-field MRI and MER can directly visualize and precisely locate the STN (12,13,17,18), but they cannot ascertain the correct region for the electrodes. Therefore, some centers use mulitple microelectrodes to delineate the STN borders during surgery for targeting precision (29). MRI-guided STN DBS without microelectrode recording can lead to substantial mean improvements in the motor disability of PD patients with improved quality of life due to its mean location errors of 1.3 mm in 79 DBS surgical cases (30). The Euclidean distances indicate that the present method has no significant difference, with this method being more robust than experts. Preoperative reconstruction using MR sequences will allow surgeons to precisely assess the positions of target structures and prepare an operation plan that reduces the repeated adjustments using intraoperative MER.

CONCLUSIONS

This paper presents an automated algorithm to segment and reconstruct the small human STN using high-field MR images. The method can effectively help surgeons directly visualize and locate the STN so that they can prepare appropriate surgery plans. The robustness and effectiveness were verified by comparisons to manual STN segmentation and reconstruction. This method for STN segmentation and reconstruction should provide an effective method for advancing STN localization and direct visualization.

Acknowledgements

This study was supported by the National Key Technology Research and Development Program (No. 2011BAI12B07) and the National Natural Science Foundation of China (Grants No. 51125028 and 51407103).

Authorship Statements

Drs. Bo Li, Luming Li, and Changqing Jiang designed and conducted the study. Drs. Jianguo Zhang and Dawei Meng collected the MRI data. All authors approved the final manuscript.

How to Cite this Article:

Li B., Jiang C., Li L., Zhang J., Meng D. 2015. Automated Segmentation and Reconstruction of the Subthalamic Nucleus in Parkinson's Disease Patients. Neuromodulation 2016; 19: 13–19

REFERENCES

1. Benabid AL, Chabardes S, Mitrofanis J et al. Deep brain stimulation of the subthalamic nucleus for the treatment of Parkinson's disease. *Lancet Neurol* 2009;8: 67–81.
2. Xiao YM, Jannin P, D'Albis T et al. Investigation of morphometric variability of subthalamic nucleus, red nucleuse and substantia nigra in advanced Parkinson's disease patients using automatic segmentation and PCA-based analysis. *Hum Brain Mapp* 2014;35:4267–4964.
3. Vayssiere N, Hemm S, Zanca M et al. Magnetic resonance imaging stereotactic target localization for deep brain stimulation in dystonic children. *Neurosurg* 2000;93:784–790.
4. Star PA, Christine CW, Theodosopoulos PV et al. Implantation of deep brain stimalators into the subthalamic nucleus: technical approach and magnetic resonance imaging-verified lead location. *J Neurosurg* 2002;97:370–387.
5. Saint JA, Hoque T, Pereira LC et al. Localization of clinically effective stimulating electrodes in the human subthalamic nucleus on magnetic resonance imaging. *Neurisurg* 2002;97:1152–1160.
6. Patel NK, Heywood K, O'Sullivan K et al. MRI-directed subthalamic nucleus surgery for Parkinson's disease. *Stereotact Funct Neurosurg* 2002;78:132–145.
7. Shen WG, Wang HY, Lin ZG et al. Stereotactic localization and visualization of the subthalamic nucleus. *Chin Med* 2009;122:2438–2443.
8. Lanotte MM, Rizzone M, Bergamasco B et al. Deep brain stimulation of the subthalamic nucleus: anatomical, neurophysiological, and outcome correlations with the effects of stimulation. *J Neurol Neurosurg Psychiatr* 2002;72:53–58.
9. Plaha P, Ben-Shlomo Y, Patel NK et al. Stimulation of the caudal zona incerta is superior to stimulation of the subthalamic nucleus in improving contralateral parkinsonism. *Brain* 2006;129:1732–1747.
10. Maks CB, Buston CR, Walter JL et al. Deep brain stimulation activation volumes and their association with neurophysiological mapping and therapeutic outcomes. *J Neurol Neurosurg Psychiatr* 2009;80:659–666.
11. Richter EO, Hoque T, Halliday W et al. Determining the position and size of the subthalamic nucleus based on magnetic resonance imaging results in patients with advanced Parkinson disease. *Neurosurg* 2004;100:541–546.
12. Wong S, Baltuch GH, Jaggi JL et al. Functional localization and visualization of the subthalamic nucleus from microelectrode recordings acquired during DBS surgery with unsupervised machine learning. *J Neural Eng* 2009;6:026006.
13. Slavin KV, Thulborn KR, Wess C et al. Direct visualization of the human subthalamic nucleus with 3T MRimaging. *Neuroradiology* 2006;27:80–84.
14. Eskandar EN, Shinobu LA, Penney LB et al. Stereotactic pallidotomy performed without using microeletrode guidance in patients with Parkinson's disease: surgical technique and 2-year results. *Neurosurg* 2000;92:375–383.
15. Aviles-Olmos I, Kefalopoulou Z, Tripoliti E et al. Long-term outcome of subthalamic nucleus deep brain stimulation form Parkinson's disease using an MRI-guided and MRI- verified approach. *J Neurol Neurosurg Psychiatr* 2014;85: 1419–1425.
16. Xiao YM, Bailey L, Chakravarty MM et al. Atlas-Based Segmentation of the Subthalamic Nucleus, Red Nucleus, and Substantia Nigra for Deep Brain Stimulation by Incorporating Multiple MRI Contrasts. Third International Conference, IPCAI 2012.
17. Cho ZH, Min HK, Oh SH et al. Direct visualization of deep brain stimulation targets in Parkinson disease with the use of 7-Tesla magnetic resonance imaging. *Neurosurg* 2010;113:639–647.
18. Patil PG, Conrad EC, Aldridge JW et al. The anatomical and electrophysiological subthalamic nucleus visualized by 3-T magnetic resonance imaging. *Neurosurg* 2012;71:1089–1095.
19. Caselles V, Kimmel R, Sapiro G. Geodesic active contours. *Int J Computer Vision* 1997;22:61–79.
20. Kimmel R, Amir A, Bruckstein AM. Finding shortest paths on surfaces using level set propagation. *IEEE Trans Pattern Anal Mach Intell* 1995;17:635–640.
21. Chan T, Vese L. Active contours without edges. *IEEE Trans Image Process* 2001;10:266–277.
22. Lankton S, Tannenbaum A. Localizing region-based active contours. *IEEE Trans Image Process* 2008;17:2029–2039.
23. Jasit SS, David LW, Swamy L. *Handbook of biomedical image analysis*, Vol. II, *Segmentation Models*. New York: Kluwer Academic/Plenum Publishers, 2005.
24. Jianping F, Guihua Z, Mathurin B et al. Seeded region growing: an extensive and comparative study. *Pattern Recogn Lett* 2005;26:1139–1156.
25. Li C, Xu C, Gui C et al. Distance regularized level set evolution and its application to image segmentation. *IEEE Trans Image Process* 2010;19:3243–3254.
26. Rouhani M, Sappa AD Implicit B-spline fitting using the 3L algorithm. 2011 18th IEEE International Conference on Image Processing (ICIP).

27. Starr PA. Placement of deep brain stimulators into the subthalamic nucleus and globus pallidus internus: technical approach. *Stereotact Funct Neurosurg* 2002;79:118–145.
28. Ellen JL, Bram P, Paul AM et al. Magnetic resonance imaging techniques for visualization of the subthalamic nucleus. *Neurosurg* 2011;115:971–984.
29. Schlaier JR, Janzen A, Fellner C. The influence of intraoperative microelectrode recordings and clinical testing on the location of final stimulation sites in deep brain stimulation for Parkinson's disease. *Acta neurochir (Wien)* 2013;155: 357–366.
30. Foltynie T, Zrinzo L, Martinez-Torres I et al. MRI-guided STN DBS in Parkinson's disease without microelectrode recording: efficacy and safety. *J Neurol Neurosurg Psychiatr* 2011;82:358–363.

